Effect of CNT addition and dispersive agents on the transport properties and microstructure of cement mortars

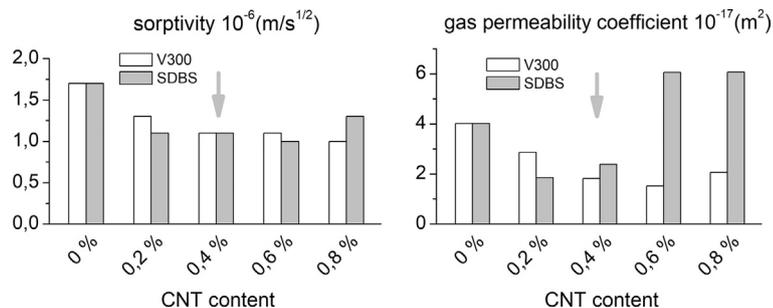P. Alafogianni [a], K. Dassios [a], C.D. Tsakiroglou [b], T.E. Matikas [a], N.M. Barkoula [a],*

[a] Department of Materials Science and Engineering, University of Ioannina, 45110 Ioannina, Greece
[b] Foundation for Research and Technology Hellas-Institute of Chemical Engineering Sciences, Stadiou Street, Platani, 26504 Patras, Greece

HIGHLIGHTS

- Mortars present a refinement of pores as a function of curing time and CNT content.
- Refinement is due to CNTs dispersion and deflocculating of cement by dispersants.
- Small amounts of CNTs (up to 0.4 wt %) are beneficial for the transport properties.
- Dispersive agents' role is crucial in controlling transport of nanomodified mortars.

GRAPHICAL ABSTRACT

ABSTRACT

The current study investigates the dependence of transport properties of carbon nanotube (CNT)-modified mortars on tube content, type of dispersive agent and microstructure. CNT addition was found to result in up to 50% reduction of sorptivity, due to the refinement of pores in the mortars. No relation was found between water absorption at equilibrium, chloride diffusion and gas permeability coefficient with CNT content, dispersive agent type and microstructural parameters. The behavior was linked with the presence of high amount of dispersive agents which, not only control the level of compaction, but also chemically interact with water or methanol altering transport.

© 2018 Elsevier Ltd. All rights reserved.

1. Introduction

It is well accepted that durability of cement-based infrastructures is highly dependent on their performance against aggressive environments and service conditions while durability improvement is of tremendous importance for the society. Due to their porous nature, cementitious materials are prone to ingress of liquids and gasses which may contain harmful substances (i.e. chlorides,

sulfates, carbon dioxide, etc) hence can compromise the materials' durability. The transport of ions, liquids and gases in porous materials can be described in different ways depending on the driving force and the nature of transport phenomena [1]. One of the main mechanisms in which fluids are absorbed and transmitted in cementitious materials, is capillary suction. Other mechanisms are permeation and diffusion. In permeation, a liquid or gas moves through a sample under a pressure gradient, while in diffusion, the motion of free molecules or ions is due to a concentration gradient [2–5]. The geometry and topology of the pore network (total porosity, pore size distribution, pore connectivity, tortuosity, etc) play a

---

* Corresponding author.
  E-mail address: nbarkoul@cc.uoi.gr (N.M. Barkoula).

key role on the transport properties and thus the durability of cementitious materials [2–6].

During the last two decades, a lot of work has focused on integrating multi-functionalities and smartness in next-generation cement composites via the incorporation of nano-fillers or fibers [7,8]. Among nano-inclusions, CNTs have attracted great scientific attention due to their unique characteristics (high electronic, magnetic and mechanical properties, high aspect ratios, etc) [7–12]. Several studies connect the mechanical performance and durability of CNT-modified cementitious composites with their microstructure, suggesting a beneficial role of CNTs in terms of reduction of porosity and pore connectivity, hydration nucleation and pore bridging [9–15]. However, to fully exploit the outstanding properties of embedded CNTs in any medium, absolute pre-requisites are their de-bundling and separation. Unfortunately, the high Van der Waals forces that act on the surface of CNTs, in combination with their high specific surface area and aspect ratios, cause their entanglement and formation of agglomerates in the presence of most common mixing solvents [16–18]. Great research efforts have focused on overcoming this issue suggesting the use of various dispersion protocols and agents [19–23]. The most common route to disperse CNTs in cementitious continuous media is the non-covalent approach where a dispersive agent (normally surfactant or plasticizer) is used as nanotube surface modifier which renders the tubes' outer walls friendly to liquid solvents hence enabling effective homogenization, usually achieved by ultrasonication [22–25]. However usage of dispersive agents is not always without side-effects to the physical properties and microstructure of cementitious hosts. For example, surfactants are known to relate to cement hydration inhibition and air entrapment [25,26]. Incorporation of de-foaming agents combined with low concentrations of surfactants, has been suggested as a countermeasure [26,27]. Another viable solution, use of cement superplasticizers as dispersive agents, may also impose restrictions due to the limitations in the amount of the superplasticizer which can be applied without deterioration of the physical properties of the cement material (workability, consistency) and without segregation.

Although microstructure and durability are related, safe assessments of the durability of CNT-modified mortars solely in terms of their microstructure is not trivial since "pure" transport properties (reflecting the pore structure) do not take into consideration the fluid-paste interactions (interaction of water, chloride binding, etc). There is thus a need of direct understanding of the effect of CNT addition on transport properties and durability of cementitious materials and this knowledge is, so far, limited [28–33]. Han et al. [28] used two different types of surfactants to disperse 0.2 wt% CNTs in mortars and investigated the transport properties of the nanomodified cementitious materials. A decrease of water sorptivity coefficient, water permeability coefficient, and gas permeability coefficient was observed after the addition of CNTs independent to the surfactant type [28]. Wang et al. discussed the chloride ion penetration, sulfate attack resistance and microstructure of CNT-modified pastes with up to 0.15 wt% CNTs concluding that 0.1 wt% provided the best resistance to both chloride and sulfate attack [29]. Similar work was performed by Lu et al. [30] who studied the chloride penetration of ultra-high strength concrete with up to 0.15 wt% CNTs and found best results at 0.05 wt%. In the same direction, Mohammed et al. [31] proved that the incorporation of graphene oxide in cement mortars improved their water sorptivity and chloride penetration while Du and Pang's study [32] revealed that the addition of graphene nano-platelets can improve the barrier properties of cement mortar by refining the pore structure. Finally, corrosion kinetics of steel reinforcement embedded in CNT-modified cement pastes was the subject of the study of Camacho et al. [33], who documented higher levels of corrosion in

aggressive environments (carbonation and chloride attacks) due to the presence of CNTs.

Existing literature reports offer scattered information in the sense that they either investigate a series of properties at limited CNT contents (up to 0.2 wt%) [28–30] or a certain property (e.g. corrosion kinetics of steel) at a wider range of contents (up to 0.5 wt%) [33]. The present is the first systematic study of the effect of CNT addition on water absorption, gas permeability and chloride penetration of CNT-modified cement mortars with tube contents of 0.2 to 0.8 wt%. The basis of the selected content range is to gain information on systems below and above the electrical percolation threshold which is normally around 0.5–0.6 wt% for this type of material [34,35].

The selection of dispersive agent for CNT contents up to 0.8 wt% is however a challenging task. As aforementioned, surfactant based suspensions are linked with side-effects on the physical properties of the cement paste even at low surfactant concentrations while superplasticizers show limited dispersion quality at low concentrations and may result in deterioration of the physical properties when their concentration exceeds a critical value (above ca. 2 wt% of cement). The current study evaluates the transport properties of CNT-modified mortars prepared using two anionic dispersive agents, Sodium Dodecyl-benzene sulfonate (SDBS) a surfactant particularly popular for CNT separation, and Viscocrete Ultra 300 (V300), a superplasticizer specific to suspensions targeted for cement-based composites. To achieve sufficient dispersion and limit any side-effect from the excessive use of the dispersive agents the SDBS/CNTs ratio is set at 0.5/1, while the corresponding ratio for V300 is 1.5/1. This selection is based on previous UV–Vis findings demonstrating that SDBS is app. 5 times more efficient in dispersing CNTs than V300 and a ratio as low as 0.5/1 is sufficient to separate the CNTs in aqueous media [22]. Furthermore, due to their large surface area, nanomaterials compromise the cement workability [36]. In order to keep the workability of all mixtures constant, different amounts of superplasticizer Viscocrete Ultra 600 (V600) are added during the preparation of each specimen. Thus the V300/CNTs ratio is restricted to 1.5/1 even if its dispersion efficiency is significantly lower than SDBS [22]. Since the maximum amount of CNTs used in the current study is 0.8 wt% of cement, applying V300/CNTs ratios higher than 1.5/1 would result in total superplasticizer quantities (applied as dispersants and workability modifiers) close to 2 wt% which is the upper limit in mortar compositions for the most commercially available superplasticizers. Thus the idea here is not to use identical dispersion/preparation conditions but to tailor the mix design to each dispersant in order to facilitate the incorporation of higher amounts of CNTs maintaining the physical properties of nanomodified mortars close to those of the plain specimens.

Based on the above, sorptivity coefficients due to capillary rise, water absorption at equilibrium, gas permeability and chloride penetration coefficients are calculated as a function of CNT content and dispersive agent. The obtained results are correlated with the pore size distributions of the investigated systems, obtained by mercury porosimetry.

2. Materials and methods

2.1. Materials, specimens preparation

Long multi-walled CNTs ("ONEX MW1000C1", Glonatech SA, Greece), synthesized via Fluidized Bed Chemical Vapor Deposition (FBCVD) were used in the present study. The physicochemical properties along with the specific surface of CNTs used in the current study are included in Table 1. CNTs were initially dispersed in water-based suspensions by aid of SDBS, Sigma-Aldrich code

Table 1
Physicochemical properties of CNTs.

Parameter	Value
Length	>10 μm
Diameter range	20–45 nm
Carbon Purity	>94%
Metal particles	<5.9%
Specific surface area [37]	>150 m^2g^{-1}
Amorphous carbon	<0.1
Bulk density	0.08–0.12 gcm^{-3}

289957, or Viscocrete Ultra 300 (V300), supplied by Sica Hellas SA. SDBS is an anionic surfactant with a relatively high critical micelle concentration value of 1.5 mM [23], while V300 is a polycarboxylate-based, chloride free, anionic polymer. In order to achieve homogeneous CNT dispersion, an optimized sonication protocol was followed using a Hielscher UP400S 24 kHz device (Hielscher Ultrasonics GmbH, Teltow, Germany), at an energy input rate of 7700 J/min based on conclusions from previous pilot studies [22,23]. SDBS/CNTs ratio was kept at 0.5/1, while the corresponding ratio for V300 was 1.5/1. CNTs were added at five contents, i.e. 0.2, 0.4, 0.6 and 0.8 wt% of cement for both dispersive agents. At the end of the sonication process, suspensions were placed in desiccators connected with a pump and vacuum was applied for 45 min to remove any residual air bubbles.

For the preparation of mortars, ordinary Portland cement - ASTM type I 42.5R (see Table 2) and sand provided by TITAN cement company S.A. were mixed according to BS EN 196-1 using a constant w/c ratio of 0.5.

During the last minute of the mixing procedure, a certain quantity of Superplasticizer Viscocrete Ultra 600 (V600), supplied by Sica Hellas SA, was used as workability modifier. In the case of surfactant-assisted suspensions, an anti-foaming agent, namely Tributyl-Phosphate (TBP), was also used. The designation, mix proportions, air content (BS-EN 1015-7) and workability (BS-EN 1015-3) of the plain and CNT-modified fresh mortars are included in Table 3. The fresh mixtures were poured in steel molds with dimensions of 160 × 40 × 40 mm^3 and specimens were demoulded after

Table 2
Composition and properties of cement.

	Value
SiO_2	21%
Al_2O_3	5%
Fe_2O_3	3%
CaO	62%
MgO	2%
SO_3	3%
K_2O	1%
Specific surface area (Blaine)	0.42 m^2g^{-1}
Initial setting (time)	150 min

24 h and stored in humid environment. In order to evaluate the effect of curing on the transport properties, two groups of specimens with 7 and 28 days of curing were created.

2.2. Water absorption and diffusion

In order to define the water absorption behavior due to capillary suction, the standard methodology described in ASTM C1585-04 was followed. To this end, 50 mm thick specimens were cut from the cured mortars using a wet saw. For pre-conditioning, specimens were placed in an environmental chamber at a temperature of 50 ± 2 °C and Relative Humidity (RH) of 80 ± 3% for 3 days. After that, specimens were placed inside a sealable container at 23 ± 2 °C for 15 days. This step provided enough time for moisture to be well distributed throughout the specimens. Afterwards, their side surfaces were sealed with 3–4 layers of plastic paint to ensure uniaxial flow of the water and their initial mass was determined. Finally the specimens were immersed in water at a depth of 3 mm using a holding device. Three specimens at each material composition were examined and the mass of the specimens was recorded at pre-determined time intervals. Absorption, i, units of m, was calculated based on equation (1):

$$i = \frac{\Delta W}{A\rho} \qquad (1)$$

where: $\Delta W = W_t - W_o$, is the change in specimen mass at the time t, in g; W_t = specimen mass at time t, in g; W_0 = initial specimen mass, in g; A = exposed area of the specimen, in m^2; ρ = density of the water, in g/m^3.

Based on the theoretical work of Hall [38,39] the absorption, i, is, for the one-dimensional case of water absorption, expressed as a function of sorptivity, S and time, t [38,39] according to Eq. (2):

$$i = B + St^{1/2} - Ct \qquad (2)$$

where: B = constant term representing the intercept at $t = 0$, in m; S = sorptivity, in $m/s^{1/2}$; C = fitting coefficient, in m/s.

As discussed previously, constant B arises from the filling of open surface porosity on the inflow surface, while during early stages of the capillary rise process most building materials obey $t^{1/2}$ law and then C becomes zero [38]. Deviation from this law implies that either the capillary gradients in the sample are as low as to be comparable with the gravitational potential (coarse pored materials), or that the porous matrix is not inert in contact with water [38,39].

Water absorption by total immersion (ΔW_e) was also defined. Specimens were first dried in an oven at 50 ± 2 °C, until a constant mass (M_d) was reached and then fully immersed in water at 23 ± 2 °C up to saturation (M_s). During this test, the change in specimen mass at equilibrium was defined according to Eq. (3):

$$\Delta W_e(\%) = \frac{W_s - W_d}{W_d} \qquad (3)$$

Table 3
Designation, mix proportions and properties of plain and CNT-modified fresh mortars (prefix V stands for V300, prefix S stands for SDBS in the designation of the samples).

Designation	Cement (g)	Water (g)	Sand (g)	CNTS (g)	V300 (g)	SDBS (g)	TBP (g)	V600 (g)	Air content (%)	Workability (cm)
Plain	450	225	1350	0	0	0	–	1.7	5.2	16.50
V0.2	450	225	1350	0.9	1.4	0	–	1.5	5.2	16.10
V0.4	450	225	1350	1.8	2.7	0	–	0.9	5.4	16.00
V0.6	450	225	1350	2.7	4.1	0	–	0.5	5.8	16.50
V0.8	450	225	1350	3.6	6.8	0	–	0.1	5.6	16.50
S0.2	450	225	1350	0.9	0	0.5	0.7	0.9	5.8	16.50
S0.4	450	225	1350	1.8	0	0.9	0.7	1.8	5.4	16.50
S0.6	450	225	1350	2.7	0	1.4	0.7	1.9	5.2	16.00
S0.8	450	225	1350	3.6	0	1.8	0.7	2.1	5.7	16.25

where: W_d = specimen dry mass, in g; W_s = specimen mass at saturation, in g; ΔW_e = relative change in specimen mass at equilibrium, in %.

2.3. Gas permeability

While water vapor permeability is more relevant to service conditions of cementitious materials, gas permeability measurements are preferred since most gases show lower interactions with cementitious matter compared to water [40,41]. Numerous gas permeability test methods can be found suggesting different pre-conditioning protocols, different permeability gases etc [42–47]. Methanol was chosen as the permeating fluid in the current study since it shows low reactivity with cement paste, it has a relatively low bowling temperature (65 °C), provides fast and credible results and it is considered suitable for cementitious mortars [28,46,47]. The testing apparatus proposed by Alshamsi and Imran [46] was adapted here. For this measurement 10 mm thick specimens were dried in an oven at 90 °C for 3 days. Specimens were periodically weighted to ensure that a constant mass was established within the timeframe of drying. Pre-conditioning (drying) was performed at a temperature below 100 °C instead of 105 °C suggested by Alshamsi et al. and other researchers [46,48] in order to avoid the development of micro-cracks in the test specimens. After drying, their dimensions were measured and they were placed on glasses filled with a small amount of methanol (15 ml). The edge of each glass was sealed with silicone at the contact point with the specimen to avoid leakage of ethanol. Each specimen was also sealed sideways to ensure unidirectional flow of the gas. The weight of specimen-glass-methanol setup was measured and recorded as initial mass. Subsequently, specimen-glass-methanol setups were placed in a water bath at 50 ± 3 °C and their mass was recorded at pre-determined time intervals. All measurements were performed in a fume hood environment. The gas permeability coefficient, k, was calculated using equation (4) which is based on Darcy's law [46]:

$$k = 2\eta \frac{L}{A} Q \frac{P_2}{P_1^2 - P_2^2} \tag{4}$$

where: k = specific gas permeability coefficient, in m^2; η = dynamic viscosity of methanol, in Ns/m^2; L = length of flow, in m; A = cross-sectional area perpendicular to the flow direction, in m^2; Q = volumetric flow rate, in m^3/s; P_1 = inlet pressure, in N/m^2; P_2 = outlet pressure, in N/m^2.

For the calculation of η, Q, P_1 and P_2 equations specific to methanol can be found elsewhere [46,47,49].

2.4. Chloride diffusion

Among the most aggressive chemical species responsible for the corrosion of steel reinforcement in cementitious materials, are chloride ions. The ions can penetrate via capillary absorption, permeation or diffusion, with the latter being the most common way for their movement. In the present study, determination of the apparent chloride diffusion coefficient was performed according to standard protocol ASTM C 1556. Unmodified and representative CNT-modified specimens (0.4 and 0.8 wt% CNTs) were exposed at a 5% NaCl solution using a salt-spray chamber for 100 days. Specimens with dimensions of 100x100x150 mm^3 were sealed sideways leaving two opposite sides exposed. After the salt-spray exposure, cylindrical cores were cut from the initial specimens in half and the depth of chloride penetration was defined after grinding at precise depth intervals of 1 mm using Profile Grinder PF-1100 purchased by Germann Instruments A/S, Denmark. The calculation of the apparent chloride diffusion coefficient was based on Fick's second law of diffusion. The values of surface concentration and apparent chloride diffusion coefficient were determined by fitting equation (5) to the measured chloride-ion contents by means of a non-linear regression analysis using the method of least squares.

$$C_{(x,t)} = C_s - (C_s - C_i)\text{erf}\left(\frac{x}{\sqrt{4tD_a}}\right) \tag{5}$$

Where: $C_{(x,t)}$ = chloride ion concentration, measured at depth $\times$ and exposure time t, in mass %; C_s = chloride ion concentration at the surface, in mass %; C_i = initial chloride ion concentration, in mass %; erf = the error function described in equation (6); x = depth below the expose surface, in m; t = exposure time, in s; D_a = apparent chloride diffusion coefficient, in m^2/s.

$$\text{erf}(z) = 2/\sqrt{\pi} \int_0^z \exp(-u^2)du \tag{6}$$

2.5. Pore size characterization

Mercury intrusion curves of the plain and CNT-modified mortars were obtained using a Quantachrome PoreMaster 60 Hg Porosimeter. The same pre-conditioning protocol as in the case of gas permeability measurements was followed here (see paragraph 2.3). A pre-weighted mass of each porous sample was placed in a penetrometer (consisting of a sample holder communicating with a capillary tube) which was inserted in the low pressure chamber of porosimeter. After having evacuated the penetrometer at pressure less than 50 mTorr, the penetrometer was filled with mercury, surrounding the evacuated porous sample, by applying an initial gas pressure of 0.1 atm. This external pressure started to increase stepwise by pressurizing gas nitrogen on the free surface of mercury left in the capillary tube of penetrometer. The volume of mercury injected in the porous sample at each pressure value was measured by detecting changes of the capacitance of the capacitor created between the mercury column and a metallic holder surrounding the penetrometer. The low pressure measurements (low pressure intrusion curve) stopped at a maximum pressure of 2.4 atm and then the system was ventilated at atmospheric pressure. Afterwards, the penetrometer was removed from low pressure chamber, weighted and transferred to the high pressure chamber where the external pressure was increased gradually from 1 atm to ~3500 atm (high pressure Hg intrusion curve), and then was decreased again to atmospheric pressure (high pressure Hg extrusion curve). Since the low pressure Hg intrusion curve may be affected drastically by non-random surface irregularities, and for the sake of comparative analysis of the internal porosity of the samples, only the high pressure Hg intrusion curves were taken in account for the computation of porosity and pore diameter distribution. The mercury penetration in a pore is governed by the Washburn equation given by [50]:

$$D = -\frac{4\gamma cos\theta}{P} \tag{7}$$

where: D = measured pore diameter, in m; γ = 0.48 (the mercury surface tension), in N/m; θ = 40 (mercury/vacuum contact angle), in °; P = external (capillary) pressure, in N/m^2.

This manner, pore diameters over the size range 0.0036–13 μm may be probed. Based on the foregoing relationship, the capillary pressure can be converted into an equivalent cylindrical pore diameter. Assuming that the pore space consists of a bundle of parallel cylindrical pores of equal length, the cumulative fraction of porosity saturated with Hg at a given pore diameter was differentiated to obtain the (volume based) pore diameter distribution (PDD) for each sample. The statistics of each PDD was quantified by their mean value, μ, and standard deviation, σ. In addition, the total pore volume (V_p) was defined and the specific surface

area (S_p) of the sample (the area of pores filled up to the minimum pore diameter probed per mass unit) was calculated by integrating the cumulative high pressure Hg intrusion curve.

3. Results

3.1. Transport properties

The effect of CNT content and dispersive agent type on water absorption behavior due to capillary suction is illustrated in Fig. 1 for early stages of curing (7 days) and Fig. 2 after 28 days of curing. As seen in Fig. 1, addition of CNTs results in the reduction of water absorption, i, due to capillary suction during the early stages of curing. The data also reveal an interesting, yet crucial, role of dispersive agent type on capillary suction, wherein V300 containing specimens present almost the same response independently of CNT content (Fig. 1b), while specimens prepared using SDBS show a considerable reduction of cumulative absorption, i, as a function of CNT content (Fig. 1a).

The beneficial role of CNTs in the reduction of capillary suction is also evident in the water absorption data after 28 days of curing, Fig. 2. As seen in Fig. 2a, in V300 containing specimens, the higher the CNT content, the lower the absorption, i. Based on Fig. 2b it is observed that i is also reduced with nanomodification when SDBS is used as dispersive agent, however the variation of i with the CNT content is not monotonic, since specimens with 0.2 and 0.4% CNTs behave similarly and the same holds for those with 0.6 and 0.8%.

Further evaluation of the experimental results presented in Figs. 1 and 2 is obtained after their fitting with equation (2), which allows the calculation of sorptivity S, constant B and coefficient C (see Table 4). Based on the obtained data, it appears that Eq. (2) describes well the cumulative capillary absorption process, with

a coefficient of determination $R^2 > 98\%$ (see Table 4). The rate of absorption, S, is substantially reduced in 7 days cured nanomodified mortars with 0.8% CNTs (up to app. 50% for both SDBS and V300 specimens). Coefficient C is quite low and considerably reduces after nanomodification (up to 80% in V300 and 40% in SDBS specimens). Compared to curing duration of 7 days, 28 days of curing is found linked to sorptivity dropping by one order of magnitude in unmodified specimens. Specimens prepared using SDBS surfactant present similar sorptivity values with those of V300, independently of CNT content. Furthermore, nanomodification results in substantial reduction of S (app. 40%), which is however slightly lower compared to the respective reduction of 7 days cured specimens (app. 50%). Coefficient C is also one order of magnitude lower after 28 days of curing and decreases with the addition of CNTs.

The response of 28-days-cured specimens after full immersion in water is illustrated in Fig. 3 where the effect of nanotubes on relative mass change is depicted for the two dispersive agent types used in the present study. Although this test does not follow any standardised methodology it has been applied before as a tool to assess the total open pore volume of cementitious materials [51,52]. It is interesting to note that in V300-prone specimens ΔW_e is slightly higher after the addition of CNTs up to 0.6 wt% and reduces at 0.8 wt% CNT. On the other hand, SDBS-containing specimens show a reduction of ΔW_e for all CNT contents. The reduction ranges between 8 and 17% while the optimal performance is noted at a CNT content of 0.2 wt%.

In order to illustrate the effect of nanomodification on the gas permeability, the cumulative mass loss of methanol as a function time for CNT-modified specimens is plotted in Fig. 4. Based on the slope of the linear part of the curve, it is possible to calculate the rate of mass loss and ultimately the specific gas permeability
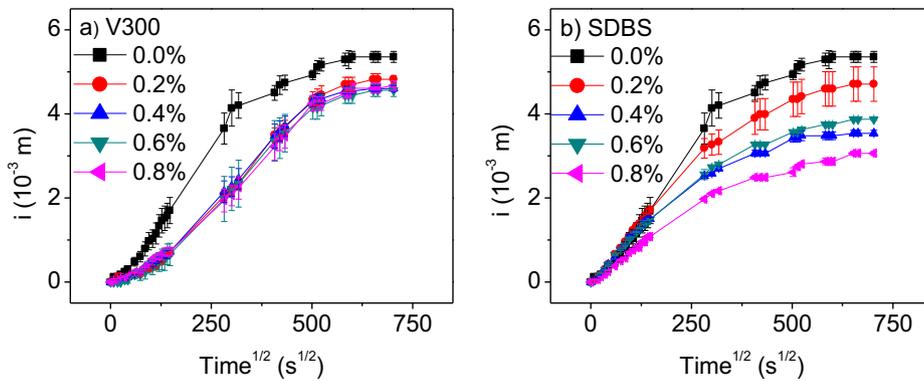

Fig. 1. Cumulative water absorption $i(t^{1/2})$ of plain and CNT-modified mortars with different dispersive agents: a) V300 and b) SDBS after 7 days of curing.
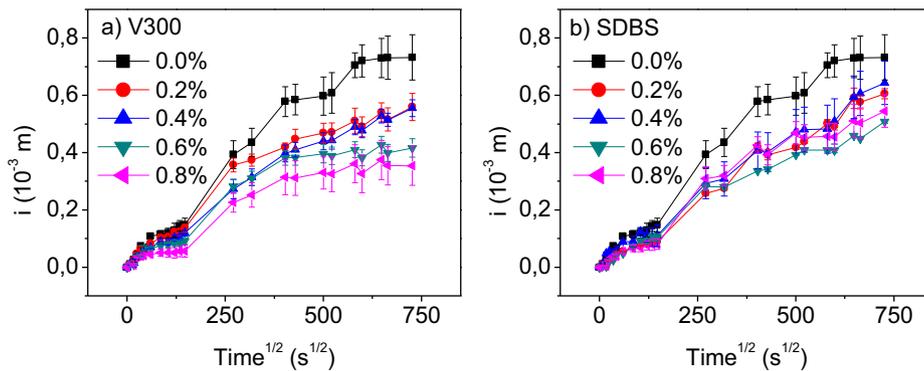

Fig. 2. Cumulative water absorption $i(t^{1/2})$ of plain and CNT-modified mortars with different dispersive agents: a) V300 and b) SDBS after 28 days of curing.

Table 4
Sorptivity (B, S and C) and permeability (k) data for plain and CNT-modified mortars prepared using different dispersive agents.

| Designation	7 days of curing				28 days of curing				
	$B\ 10^{-3}$ (m)	$S\ 10^{-6}$ (m/s$^{1/2}$)	$C\ 10^{-9}$ (m/s)	R^2	$B\ 10^{-3}$ (m)	$S\ 10^{-6}$ (m/s$^{1/2}$)	$C\ 10^{-9}$ (m/s)	R^2	$k\ 10^{-17}$ (m^2)
Plain	−0.3905	17.4	10	0.99	−0.0144	1.7	0.8	0.99	4.02
V0.2%	−0.4016	9.9	2	0.98	0.0021	1.3	0.7	0.99	2.87
V0.4%	−0.4194	10.7	4	0.98	−0.0036	1.1	0.5	1.00	1.82
V0.6%	−0.4344	10.1	3	0.98	−0.0061	1.1	0.7	0.98	1.52
V0.8%	−0.3044	9.3	2	0.99	−0.0148	1.0	0.6	0.98	2.07
S0.2%	−0.1306	14.2	10	1.00	−0.0189	1.1	0.3	0.99	1.85
S0.4%	−0.0048	11.4	9	1.00	0.0037	1.1	0.4	0.99	2.39
S0.6%	−0.0307	11.6	9	1.00	−0.0084	1.0	0.4	0.99	6.06
S0.8%	−0.0679	8.7	6	1.00	−0.0244	1.3	0.6	0.99	6.07
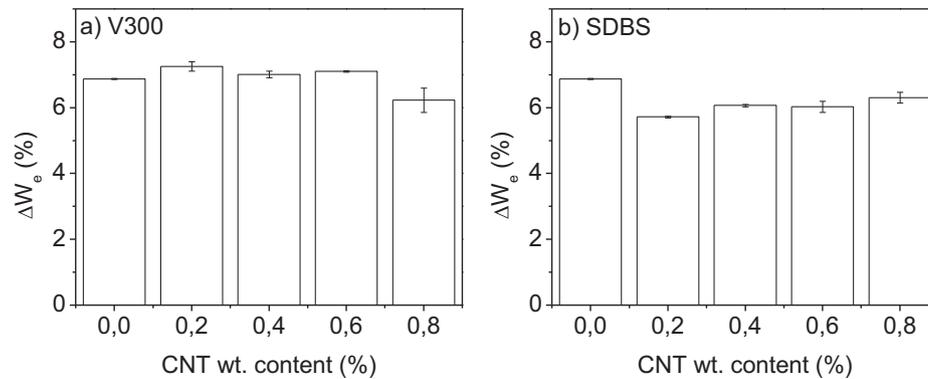
Fig. 3. Relative mass change at equilibrium ΔW_e of plain and CNT-modified mortars with different dispersive agents: a) V300 and b) SDBS after 28 days of curing.
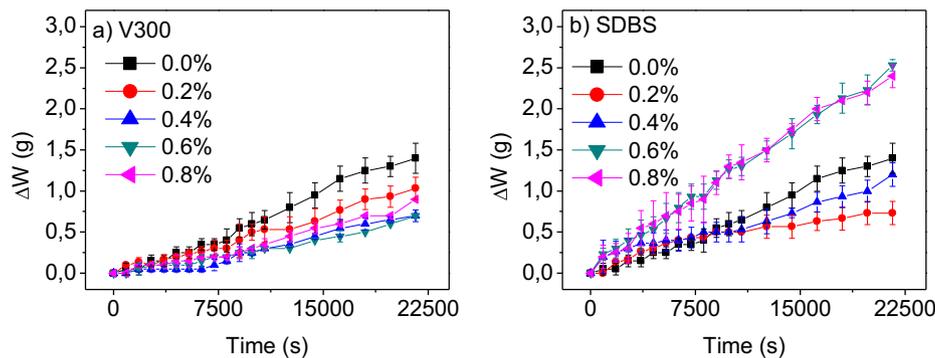

Fig. 4. Cumulative mass loss of methanol $\Delta W(t)$ after 28 days of curing for plain and CNT- modified mortars with different dispersive agents: a) V300 and b) SDBS.

coefficient, k, as described in section 2.3 (see Table 4). It is observed that methanol mass loss is considerably reduced after the addition of up to 0.6 wt% CNTs in specimens prepared using V300 as dispersive agent (Fig. 4a). On the other hand, SDBS-prone specimens present a reduction of mass loss only for CNT contents up to 0.4%. Similar observations can be made on the specific gas permeability coefficient, k, which shows a reduction of up to 62% in V300-containing specimens, while the respective reduction for SDBS-containing ones is approximately 55% for CNT contents up to 0.4 wt%. Addition of higher amounts of CNTs results in up to 50% higher k values, compared to plain specimens.

Fig. 5a illustrates the effect of CNT addition on the apparent chloride diffusion coefficient, D_a while Fig. 5b on the chloride critical depth. The latter is the penetration depth where chlorides reach the critical value of 0.05% Cl$^-$, below which there is no threat on the material's durability [53,54]. As observed, the apparent chloride diffusion coefficient is not significantly influenced by the addition of CNTs when V300 is used as dispersive agent, while specimens with SDBS show an up to app. 20% reduction of D_a,

which is more evident at 0.4 wt% CNTs. At the same time, the chloride critical depth remains almost unaffected with variations lying within standard experimental error.

3.2. Porosity and pore size distribution

In order to access the microstructure of plain and CNT-modified mortars, critical porosimetry data are presented in Table 5 while the PDD of the tested specimens is illustrated in Fig. 6.

As observed in Table 5, V_p, porosity and μ are reduced after the introduction of CNTs, while S_p increased. When V300 is used as dispersive agent, porosity shows a reduction of up to 25% at 0.6 wt% content, while μ presents an up to 63% decrease at 0.2 wt% CNTs. Highest reduction of porosity (44%) in SDBS-containing specimens is found at 0.8 wt% CNTs while respective reduction of μ (approximately 56%), is found at 0.6 wt% CNTs. Furthermore, all PDD spectra present several peaks in two separate areas; the first is the region of pore sizes smaller than 30 nm, while the second corresponds to sizes between 30 nm and 10 µm (see Fig. 6).
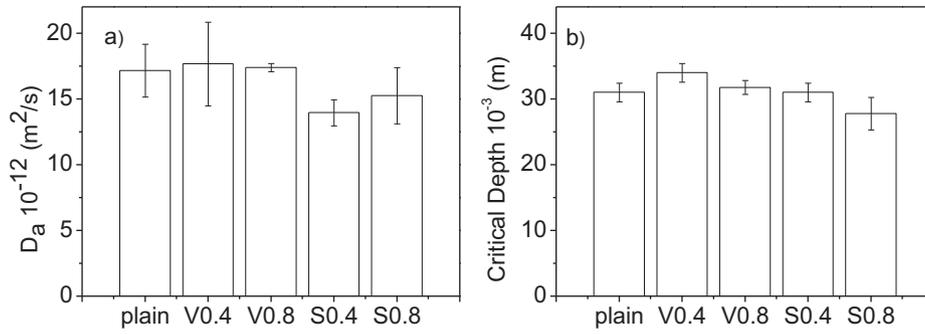
Fig. 5. Effect of CNT addition on: a) apparent chloride diffusion coefficient, D_a and b) chloride critical depth of mortars after 28 days of curing.

Table 5
Porosimetry data for plain and CNT-modified mortars prepared using different dispersive agents.

Designation	V_p (cm^3/g)	S_p (m^2/g)	Porosity (%)	μ (μm)	σ (μm)
Plain	0.060	9.31	14.59	0.091	5.28
V0.2%	0.053	17.93	10.56	0.033	7.03
V0.4%	0.048	13.94	11.67	0.042	6.26
V0.6%	0.053	15.14	10.91	0.040	6.05
V0.8%	0.052	19.41	13.83	0.036	7.90
S0.2%	0.052	12.17	11.08	0.049	6.62
S0.4%	0.056	16.39	13.39	0.040	6.77
S0.6%	0.055	15.79	10.49	0.040	6.25
S0.8%	0.046	12.53	8.06	0.051	7.00

CNT-modified specimens show a larger population in the first area, and smaller population in the second one compared to plain specimens.

Since the fraction of small to large pores or the fraction of capillary pores and their connectivity are considered more relevant than the total pore volume for the transport properties of cementitious materials [48,55–58], the results presented in Fig. 6 are further analyzed and the fraction of porosity of plain and CNT-modified specimens is calculated as a function of pore diameter. Pore sizes are divided in three distinctive areas – small (gel) pores with pore diameters between 2.5 and 10 nm, medium capillaries with pore diameters between 10 and 50 nm and large capillary pores with diameters between 50 and 10000 nm [55]. This division has been made on the basis that gel pores do not influence permeability, while capillary pores affect both permeability and transport properties. The fraction of porosity in these three distinctive areas as a function of CNT content and dispersive agent is illustrated in Fig. 7. As observed, the fraction of gel pores increases with the addition of higher amounts of CNTs. Maximum fraction of gel pores (approximately 50%) is found in V300-based specimens with
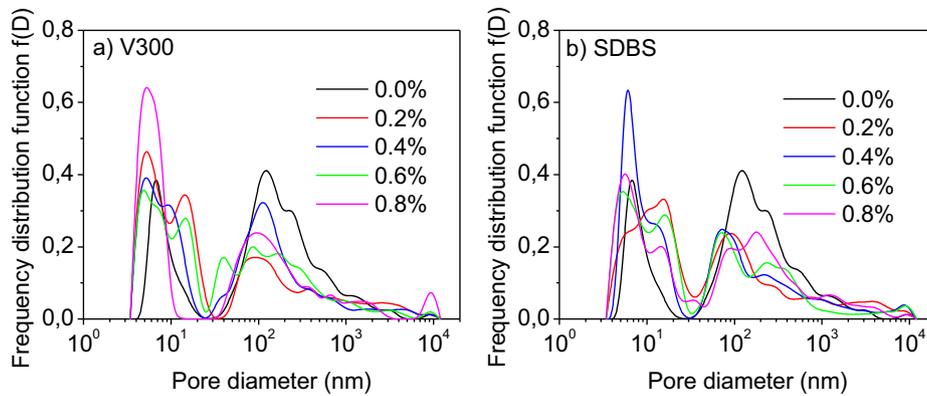

Fig. 6. Comparison of the PDD of plain and CNT-modified mortars with different dispersive agents: a) V300 and b) SDBS after 28 days of curing.
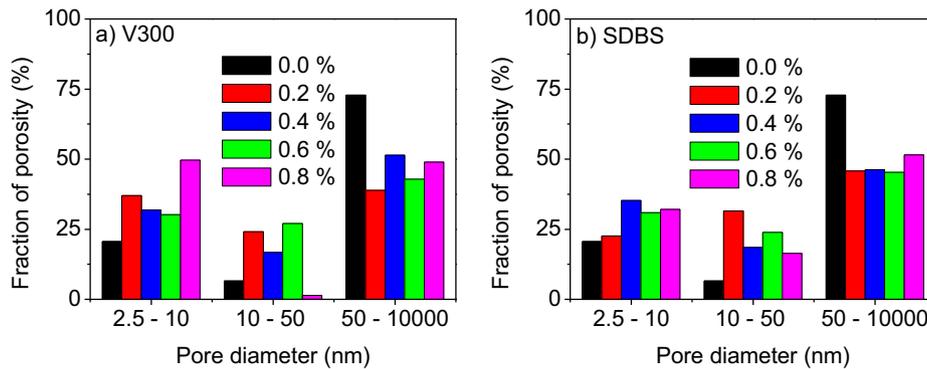

Fig. 7. Fraction of porosity at three distinctive capillary areas of plain and CNT-modified mortars with different dispersive agents: a) V300 and b) SDBS after 28 days of curing.

0.8 wt% CNTs while the respective fraction for SDBS specimens (approximately 35%) is found at 0.4 wt% CNTs. The fraction of medium sized capillary pores presents a great variation after the addition of CNTs, being overall higher than that of plain specimens. Finally, a great reduction of the large-sized capillary pores is found after the addition of CNTs from app. 73% (plain specimen) down to 38% for V300 containing specimens and 45% for those with SDBS. The fraction of large pores varies with CNT content in V300-based specimens, while it remains almost unaffected in SDBS ones for up to 0.6 wt CNTs.

4. Discussion

In order to seed light into the results presented in the previous section an attempt is made to discuss the effect of nanomodification, with the aid of dispersants, first on the microstructure and then on the transport properties of the prepared nanocomposites. Furthermore effort is undertaken to investigate potential correlations between transport properties and critical system parameters (e.g. mix design, age of curing, PDD parameters). It is important to keep in mind that the PDD data presented in Figs. 6 and 7 and Table 5 are not absolute due to limitations of the mercury intrusion porosimetry (MIP) methodology. These are mainly related to the ability of MIP to provide actual pore size distribution data, next to the fact that MIP results are greatly influenced by factors such as contact angle, surface tension, sample-drying method, sample preparation, etc [59–61]. Thus instead of trying to establish universal property-microstructure relations the discussion here is limited in making comparative assessments of the pore refinements of the investigated systems [59].

4.1. Effect of nanomodification on the microstructure

The data presented in Figs. 6 and 7 suggest a shift to finer pore sizes and a more compact microstructure in nanomodified mortars compared with plain specimens, as illustrated by the reduction of μ, V_p and % porosity and the respective increase of the S_p and fraction of mesopores (size less than 50 nm [9]). This finding is in agreement with previous observations and can be linked with CNT's ability to fill the pores between the hydration products [8–15,36,62,63]. CNTs could also contribute to the increased fraction of lower range pores by their porosity. Due to their shape, multiwalled CNTs present inner hollow cavities (mainly 3–4 nm) and aggregated pores (10 – 40 nm), formed by the interaction of isolated CNTs [64] which could explain the increased fraction of mesopores in the nanomodified mortars.

When comparing the microstructure of nanomodified mortars prepared using the different agents it is observed that the dispersion of CNTs with the aid of V300 results to greater shift from large capillary pores to gel pores compared to SDBS specimens where capillaries move from large to medium size and lesser to gel pores (Fig. 7). SDBS is an amphiphilic molecule consisting of a hydrophilic sulfonate head-group and a hydrophobic alkylbenzene tail-group which is responsible for its high dispersion ability [65,66]. Thus, next to the filling effect, high amount of isolated CNTs in the nanomodified SDBS mortars could explain the shift from large to medium sized pores. On the other hand, V300 belongs to the family of polycarboxylate-based superplasticizers, which are macromolecular surfactants consisting of an anionic backbone and non-ionic side chains [67,68]. While the anionic backbone is considered more effective in dispersing carbon-based nanoinclusions in aqueous solutions, the non-ionic side chains make also a contribution which becomes more significant at increased superplasticizer's concentration [67]. As discussed in the introduction, for the specific dispersion conditions used here, previous studies

demonstrated that SDBS is app. 5 times more efficient than V300 in dispersing CNTs in aqueous solutions [22]. This tremendous difference is nevertheless not reflected in the microstructure of the nanomodified mortars.

Apart from the efficiency of the agents in dispersing CNTs, another key aspect that needs to be addressed relates to the admixtures used in the preparation of the two classes of nanomodified mortars, their potential interaction with the cementitious matrix and in turn their impact on the microstructure. SDBS is linked with entrained air in cementitous materials, detected as voids with sizes above 10 μm [69]. Although voids of this size could not be observed in the porosimetry data (outside from the measurement range), air content results, presented in Table 3, suggest that the addition of the defoaming agent as well as the degassing process of the suspensions regulate the entrained air leading in similar air content values between plain and SDBS nanomodified mortars. On the other hand, a closer look into the composition of the V300 specimens reveals that the total quantity of polycaboxylate-based superplasticiers (either in the form of dispersive agent, i.e. V300 or as workability modifier, i.e. V600) is 2–3 time higher than that used in SDBS specimens (applied only in the form of workability modifier, i.e. V600) (see Table 3). Superplasticizers are known to influence the pore structure of cementitious materials by changing the flocculation microstructure of cement, altering the hydration process and filling pores and cracks in transition zones [70,71]. It has been documented that the use of polycarboxylate-based superplasticizers results in improved hydration and higher amount of gel pores after 7 days of curing and reduction of the total porosity and respective increase of the mesopores in 28 days cured cementitious mortars [70,72]. This explains why V300 samples present a significant reduction of the large sized pores in favor of gel pores. Thus, the refinement of pores in the prepared nanocomposites cannot be solely attributed to the presence of individual CNTs and the possible filling of the pores, and should be also linked with the presence of high amount of plasticizer in the material, which results in the production of a more compact material.

In terms of the effect of CNT content on the microstructure of the nanomodified mortars it can be concluded that the addition of 0.2 wt% is sufficient to reduce the fraction of large capillaries by 25–30% in SDBS and V300 specimens, while higher amounts of CNTs result in non-monotonic variation of large capillary pores, especially in V300 specimens, confirming the existence of a coupled effect between CNTs dispersion and deflocculating of cement by dispersing agents.

4.2. Effect of nanomodification on the transport properties and correlation with system parameters

The data presented in Figs. 1-2 and Table 4 suggest a great reduction of i, S, C after nanomodification in both 7 and 28 days cured specimens, but the evolution of studied properties with CNT content, age of curing and dispersive agent type is not monotonic. Attempts to relate sorptivity with the fraction of pores (presented in Fig. 7), V_p and % porosity (presented in Table 5) and all other measures of the soprtivity experiment (i, C) show weak or even no correlation. In the past S has been associated with the pore size and size distribution of the material since they depend on both the capillary pressure and effective porosity [2,73]. However, it is not straightforward to find the appropriate measure that represents pore size in the case of a real system, since as observed in Fig. 6, and verified in Table 5 by the high values of σ, all measured PDDs are multi-modals over a broad pore size range. Thus μ may be regarded as a measure of the position of each PDD, rather than representative of the most frequent pore size probed.

Instead of selecting an arbitrary pore size, an attempt is made to associate the sorptivity, S, after 7 and 28 days of curing, with the CNT content and critical PDD parameters including S_p, μ, and % fraction of gel pores. As observed in Fig. 8, in both 7 and 28 days cured specimens, there is quite some scatter in the variation of S with the aforementioned parameters. The general trend is that S exhibits an initial drop up to a certain value of CNT content (8a), S_p (8b) and fraction of gel pores (8d) and then stabilizes. The cutoff point of this drop is found at 0.2–0.4 wt% CNTs, $S_p \sim 12$ m^{2}g^{-1}, and fraction of gel pores $\sim$30%. On the other hand Fig. 8c demonstrates an increasing trend between S and μ in both V300- and SDBS-containing specimens, which was expected since μ represents the shift from bigger to smaller pores in the nano-modified mortars. Overall it can be concluded that, in line with the observations of § 4.1, a small amount of CNTs, as low as 0.2%, results in significant pore structure refinement which greatly affect transport due to sorptivity.

Efforts to correlate the change in mass at equilibrium, ΔW_e, with experimentally assessed properties from the sorptivity test as well as microstructural parameters (PDD) indicate no clear association. After full immersion it is observed in Fig. 3 that ΔW_e is slightly higher in nanomodified V300 specimens (apart from those with 0.8 wt% CNTs) while SDBS containing specimens show a minor reduction of ΔW_e which however diminishes as the CNT content increases. Although the original idea was to use this test as a tool to assess the total open pore volume [51,52], due to the high amount of admixtures (see Table 3), it seems that water transport takes place also through interaction between water and reactive groups of the admixtures (for instance polar groups), and not only via capillary suction. As discussed in § 4.1 SDBS contains a hydrophilic sulfonate head-group which may interact with water through hydrogen bonds [69]. Polycarboxylate-based superplasticizers possess also high polarity hydroxyl- and carboxyl- groups that show affinity to water [67]. Thus nanomodification, with the aid of dispersants, results in two competitive mechanisms here,

i.e. reduction of water absorption due to capillary suction associated with the pore refinement of the system and increase of contained water through interaction associated with the high amount of dispersive agents, and their affinity with water. It is important to note that water/dispersive agent interactions may also take place during the sorptivity test which could explain some of the discrepancies found in i and C, as a function of dispersive agent and CNT content. However due to the partial immersion of the samples the driving force of the transport is capillary.

Similar observations can be made when looking into the gas permeability results and trying to associate specific gas permeability coefficient, k, with microstructural parameters. The reduction of permeability as a function of CNT content (up to 0.6 wt%) presented in Fig. 4 can be associated with the pore refinement in V300 specimens in line with previous experimental and modeling studies [74,75]. On the other hand SDBS specimens are less permeable for up to 0.4 wt% CNT contents while at higher CNT contents permeability drastically increases. Since all SDBS nanomodified mortars present a considerable pore refinement this result cannot be associated with the pore structure of the system and should be linked with its mix design. SDBS is a relatively small molecule and the same holds for methanol. It is therefore speculated that the increased amount of SDBS as CNT content increases allows methanol to pass through the sites of the specimen where SDBS arrests. Finally, in terms of chloride ions ingress, the obtained results are not conclusive and a more systematic study is required in order to find correlations between microstructure, electrical conductivity and chloride diffusion coefficient.

5. Conclusions

The current study investigates two critical problems concerning the durability of CNT-modified cement mortars. The first is the
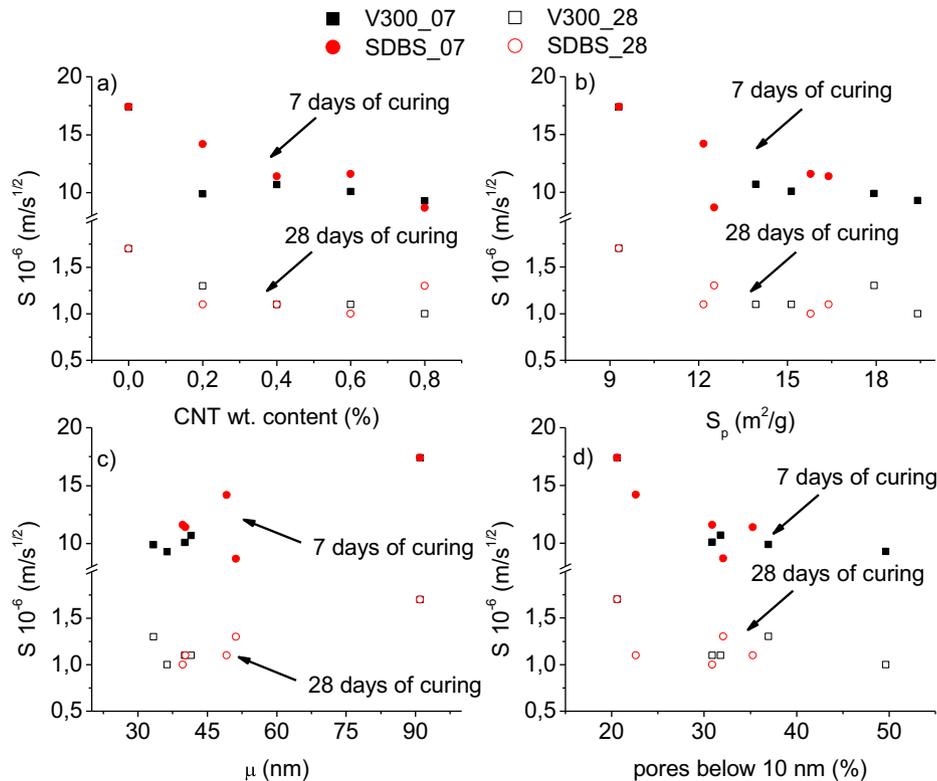

Fig. 8. Correlation between sorptivity and: a) CNT content, b) pores specific surface area, S_p, c) μ, d) fraction of pores below 10 nm (gel pores) of plain and modified mortars with different dispersive agents and CNT contents after 28 days of curing.

dependence of transport properties on CNT content and dispersive agents and the second is the correlation of transport properties with the microstructure of CNT-modified mortars. Two types of agents, an anionic surfactant (SDBS) and a plasticizer-type dispersant (V300), assisted the dispersion of CNTs at concentration of 0.2–0.8 by percent weight of cement.Transport properties are defined by measuring the sorptivity coefficients, water absorption, gas permeability and chloride penetration coefficients, while porosity and pore size distribution data are obtained from mercury intrusion curves. Based on the obtained results the following conclusions can be drawn:

- The refinement of pores in the nanomodified mortars is due to a coupled effect between CNTs dispersion and deflocculating of cement by dispersive agents.
- Nanomodification, with the aid of dispersants, results in two competitive mechanisms in terms of transport, i.e. a) reduction of absorption due to capillary suction associated with the pore refinement of the system and b) increase of absorption due to interaction between transport media and reactive groups of the admixtures.

Since transport properties of nanomodified mortars are system dependent, the amount of dispersive agents (and other admixtures) used to facilitate nanomodification and their affinity with transport media should be considered when designing new cementitious materials. In the specific systems studied here a small amount of CNTs, as low as 0.2–0.4 wt%, dispersed with the aid of V300 or SDBS, is beneficial for the transport properties since it results in reduced soprtivity and gas permeability.

Conflict of interest

None.

Funding

References

[1] V. Baroghel-Bouny, Water, vapour sorption experiments on hardened cementitious materials. Part II: essential tool for assessment of transport properties and for durability prediction, Cem. Concr. Res. 37 (3) (2007) 438–454.
[2] J. Castro, D. Bentz, J. Weiss, Effect of sample conditioning on the water absorption of concrete, Cem. Concr. Compos. 33 (8) (2011) 805–813.
[3] E.J. Garboczi, Permeability, diffusivity, and microstructural parameters: a critical review, Cem. Concr. Res. 20 (4) (1990) 591–601.
[4] Y. Zhang, M. Zhang, Transport properties in unsaturated cement-based materials – a review, Constr. Build. Mater. 72 (2014) 367–379.
[5] R. Henkensiefken et al., Water absorption in internally cured mortar made with water-filled lightweight aggregate, Cem. Concr. Res. 39 (10) (2009) 883–892.
[6] Saeidpour, M., Experimental studies of sorption and transport of moisture in cement based materials with supplementary cementitious materials, in Faculty of engineering, Division of Building Materials, 2015, Lund University: Printed in Sweden by Media-Tryck, Lund University. p. 60.
[7] B. Han et al., Smart concretes and structures: a review, J. Intell. Mater. Syst. Struct. 26 (11) (2015) 1303–1345.
[8] B. Han et al., Review of nanocarbon-engineered multifunctional cementitious composites, Compos. A Appl. Sci. Manuf. 70 (2015) 69–81.
[9] S. Parveen, S. Rana, R. Fangueiro, A Review on Nanomaterial Dispersion, Microstructure, and Mechanical Properties of Carbon Nanotube and Nanofiber Reinforced Cementitious Composites, J. Nanomater. 2013 (2013) 19.
[10] T. Manzur, N. Yazdani, M.A.B. Emon, Potential of Carbon Nanotube Reinforced Cement Composites as Concrete Repair Material, J. Nanomater. 2016 (2016) 10.
[11] S.J. Chen et al., Carbon nanotube–cement composites: a retrospect, IES J. Part A: Civ. Struct. Eng. 4 (4) (2011) 254–265.
[12] Q. Li, J. Liu, S. Xu, Progress in Research on Carbon Nanotubes Reinforced Cementitious Composites, Adv. Mater. Sci. Eng. 2015 (2015) 16.
[13] T. Nochaiya, A. Chaipanich, Behavior of multi-walled carbon nanotubes on the porosity and microstructure of cement-based materials, Appl. Surf. Sci. 257 (6) (2011) 1941–1945.
[14] B. Zou et al., Effect of ultrasonication energy on engineering properties of carbon nanotube reinforced cement pastes, Carbon 85 (2015) 212–220.
[15] G.I. Yakovlev et al., Modification of Cement Matrix Using Carbon Nanotube Dispersions and Nanosilica, Procedia Eng. 172 (2017) 1261–1269.
[16] L.A. Girifalco, M. Hodak, R.S. Lee, Carbon nanotubes, buckyballs, ropes, and a universal graphitic potential, Phys. Rev. B 62 (19) (2000) 13104–13110.
[17] N. Grossiord et al., Time-Dependent Study of the Exfoliation Process of Carbon Nanotubes in Aqueous Dispersions by Using UV−Visible Spectroscopy, Anal. Chem. 77 (16) (2005) 5135–5139.
[18] P.J.F. Harris, Carbon nanotube composites, Int. Mater. Rev. 49 (1) (2004) 31–43.
[19] X. Fu et al., Quantitative evaluation of carbon nanotube dispersion through scanning electron microscopy images, Compos. Sci. Technol. 87 (2013) 170–173.
[20] I. Madni et al., Mixed surfactant system for stable suspension of multiwalled carbon nanotubes, Colloids Surf., A 358 (1) (2010) 101–107.
[21] J. Rausch, R.-C. Zhuang, E. Mäder, Surfactant assisted dispersion of functionalized multi-walled carbon nanotubes in aqueous media, Compos. A Appl. Sci. Manuf. 41 (9) (2010) 1038–1046.
[22] P. Alafogianni et al., On the efficiency of UV–vis spectroscopy in assessing the dispersion quality in sonicated aqueous suspensions of carbon nanotubes, Colloids Surf., A 495 (2016) 118–124.
[23] K.G. Dassios et al., Optimization of Sonication Parameters for Homogeneous Surfactant-Assisted Dispersion of Multiwalled Carbon Nanotubes in Aqueous Solutions, J. Phys. Chem. C 119 (13) (2015) 7506–7516.
[24] S. Musso et al., Influence of carbon nanotubes structure on the mechanical behavior of cement composites, Compos. Sci. Technol. 69 (11) (2009) 1985–1990.
[25] H. Shao et al., Influence of dispersants on the properties of CNTs reinforced cement-based materials, Constr. Build. Mater. 131 (2017) 186–194.
[26] A. Sobolkina et al., Dispersion of carbon nanotubes and its influence on the mechanical properties of the cement matrix, Cem. Concr. Compos. 34 (10) (2012) 1104–1113.
[27] B. Wang, Y. Han, S. Liu, Effect of highly dispersed carbon nanotubes on the flexural toughness of cement-based composites, Constr. Build. Mater. 46 (2013) 8–12.
[28] B. Han et al., Transport Properties of Carbon-Nanotube/Cement Composites, J. Mater. Eng. Perform. 22 (1) (2013) 184–189.
[29] B.-M. Wang et al., Preparation and Durability of Cement-Based Composites Doped with Multi-Walled Carbon Nanotubes, Nanosci. Nanotechnol. Lett. 7 (5) (2015) 411–416.
[30] L. Lu, D. Ouyang, W. Xu, Mechanical Properties and Durability of Ultra High Strength Concrete Incorporating Multi-Walled Carbon Nanotubes, Materials 9 (6) (2016) 419.
[31] A. Mohammed et al., Incorporating graphene oxide in cement composites: a study of transport properties, Constr. Build. Mater. 84 (2015) 341–347.
[32] H. Du, S.D. Pang, Enhancement of barrier properties of cement mortar with graphene nanoplatelet, Cem. Concr. Res. 76 (2015) 10–19.
[33] M.d.C. Camacho et al., Mechanical Properties and Durability of CNT Cement Composites, Materials 7 (3) (2014) 1640–1651.
[34] A.-D. Ali et al., Electrical percolation threshold of cementitious composites possessing self-sensing functionality incorporating different carbon-based materials, Smart Mater. Struct. 25 (10) (2016) 105005.
[35] P.T. Dalla et al., Carbon nanotubes and nanofibers as strain and damage sensors for smart cement, Mater. Today Commun. 8 (2016) 196–204.
[36] S. Chuah et al., Nano reinforced cement and concrete composites and new perspective from graphene oxide, Constr. Build. Mater. 73 (2014) 113–124.
[37] F. Giannakopoulou et al., Characterization of multi-walled carbon nanotubes and application for Ni2+ adsorption from aqueous solutions, Desalin. Water Treat. 57 (25) (2016) 11623–11630.
[38] C. Hall, T.K.-M. Tse, Water movement in porous building materials—VII. The sorptivity of mortars, Build. Environ. 21 (2) (1986) 113–118.
[39] C. Hall, Water sorptivity of mortars and concretes: a review, Mag. Concr. Res. 41 (147) (1989) 51–61.
[40] V. Picandet, A. Khelidj, H. Bellegou, Crack effects on gas and water permeability of concretes, Cem. Concr. Res. 39 (6) (2009) 537–547.
[41] H. Ranaivomanana et al., Toward a better comprehension and modeling of hysteresis cycles in the water sorption–desorption process for cement based materials, Cem. Concr. Res. 41 (8) (2011) 817–827.
[42] R. Li et al., Influence of silica-based hybrid material on the gas permeability of hardened cement paste, IOP Conference Series: Materials Science and Engineering 182 (1) (2017) 012043.
[43] A. Dinku, H.W. Reinhardt, Gas permeability coefficient of cover concrete as a performance control, Mater. Struct. 30 (7) (1997) 387.
[44] H. Loosveldt, Z. Lafhaj, F. Skoczylas, Experimental study of gas and liquid permeability of a mortar, Cem. Concr. Res. 32 (9) (2002) 1357–1363.
[45] R.J. Torrent, A two-chamber vacuum cell for measuring the coefficient of permeability to air of the concrete cover on site, Mater. Struct. 25 (6) (1992) 358–365.
[46] A.M. Alshamsi, H.D.A. Imran, Development of a permeability apparatus for concrete and mortar, Cem. Concr. Res. 32 (6) (2002) 923–929.
[47] Z. Yang et al., A self-healing cementitious composite using oil core/silica gel shell microcapsules, Cem. Concr. Compos. 33 (4) (2011) 506–512.

[48] L. Bágel, V. Živica, Relationship between pore structure and permeability of hardened cement mortars: on the choice of effective pore structure parameter, Cem. Concr. Res. 27 (8) (1997) 1225–1235.

[49] R.K. Dhir, P.C. Hewlett, Y.N. Chan, Near surface characteristics of concrete: intrinsic permeability, Mag. Concr. Res. 41 (147) (1989) 87–97.

[50] E.W. Washburn, The Dynamics of Capillary Flow, Phys. Rev. 17 (3) (1921) 273–283.

[51] G. De Schutter, K. Audenaert, Evaluation of water absorption of concrete as a measure for resistance against carbonation and chloride migration, Mater. Struct. 37 (9) (2004) 591.

[52] J.M. Khatib, R.M. Clay, Absorption characteristics of metakaolin concrete, Cem. Concr. Res. 34 (1) (2004) 19–29.

[53] U. Angst et al., Critical chloride content in reinforced concrete — A review, Cem. Concr. Res. 39 (12) (2009) 1122–1138.

[54] Yi-Wei Lin, A.S.L.W., M.I. Jason, Durability Properties of Sprayed Engineered Cementitious Composite. Mater. J. 110(5).

[55] P. Pipilikaki, M. Beazi-Katsioti, The assessment of porosity and pore size distribution of limestone Portland cement pastes, Constr. Build. Mater. 23 (5) (2009) 1966–1970.

[56] H. Zhao et al., Influence of Pore Structure on Compressive Strength of Cement Mortar, Scientific World J. 2014 (2014) 12.

[57] C.C. Yang, S.W. Cho, L.C. Wang, The relationship between pore structure and chloride diffusivity from ponding test in cement-based materials, Mater. Chem. Phys. 100 (2) (2006) 203–210.

[58] J.M. Khatib, P.S. Mangat, Absorption characteristics of concrete as a function of location relative to casting position, Cem. Concr. Res. 25 (5) (1995) 999–1010.

[59] H. Ma, Mercury intrusion porosimetry in concrete technology: Tips in measurement, pore structure parameter acquisition and application, J. Porous Mater. 21 (2) (2014) 207–215.

[60] C. Gallé, Effect of drying on cement-based materials pore structure as identified by mercury intrusion porosimetry: a comparative study between oven-, vacuum-, and freeze-drying, Cem. Concr. Res. 31 (10) (2001) 1467–1477.

[61] R.A. Cook, K.C. Hover, Mercury porosimetry of hardened cement pastes, Cem. Concr. Res. 29 (6) (1999) 933–943.

[62] G.Y. Li, P.M. Wang, X. Zhao, Mechanical behavior and microstructure of cement composites incorporating surface-treated multi-walled carbon nanotubes, Carbon 43 (6) (2005) 1239–1245.

[63] S. Xu, J. Liu, Q. Li, Mechanical properties and microstructure of multi-walled carbon nanotube-reinforced cement paste, Constr. Build. Mater. 76 (2015) 16–23.

[64] Q.-H. Yang et al., Adsorption and capillarity of nitrogen in aggregated multi-walled carbon nanotubes, Chem. Phys. Lett. 345 (1) (2001) 18–24.

[65] M. Suttipong et al., Role of Surfactant Molecular Structure on Self-Assembly: Aqueous SDBS on Carbon Nanotubes, J. Phys. Chem. C 115 (35) (2011) 17286–17296.

[66] M. Adresi et al., Determining the Surfactant Consistent with Concrete in order to Achieve the Maximum Possible Dispersion of Multiwalled Carbon Nanotubes in Keeping the Plain Concrete Properties, Journal of Nanotechnology 2016 (2016) 9.

[67] Z.S. Metaxa, Polycarboxylate based superplasticizers as dispersant agents for exfoliated graphene nanoplatelets reinforcing cement based materials, J. Eng. Sci. Technol. Rev. 8 (5) (2015) 1–5.

[68] R.J. Flatt et al., Conformation of Adsorbed Comb Copolymer Dispersants, Langmuir 25 (2) (2009) 845–855.

[69] E.-S. Negim et al., Effects of Surfactants on the Properties of Mortar Containing Styrene/Methacrylate Superplasticizer, Scientific World J. 2014 (2014) 10.

[70] Y. Zhang, X. Kong, Influences of superplasticizer, polymer latexes and asphalt emulsions on the pore structure and impermeability of hardened cementitious materials, Constr. Build. Mater. 53 (2014) 392–402.

[71] J.M. Khatib, P.S. Mangat, Influence of superplasticizer and curing on porosity and pore structure of cement paste, Cem. Concr. Compos. 21 (5) (1999) 431–437.

[72] H. Huang et al., Improvement on microstructure of concrete by polycarboxylate superplasticizer (PCE) and its influence on durability of concrete, Constr. Build. Mater. 110 (2016) 293–299.

[73] S.P. Zhang, L. Zong, Evaluation of Relationship between Water Absorption and Durability of Concrete Materials, Adv. Mater. Sci. Eng. 2014 (2014) 8.

[74] Z. Lafhaj et al., Correlation between porosity, permeability and ultrasonic parameters of mortar with variable water/cement ratio and water content, Cem. Concr. Res. 36 (4) (2006) 625–633.

[75] C. Gallé, J.F. Daian, Gas permeability of unsaturated cement-based materials: application of a multi-scale network model, Mag. Concr. Res. 52 (4) (2000) 251–263.